Full-wave finite-difference time-domain simulation of electromagnetic cloaking structures

Yan Zhao*, Christos Argyropoulos, and Yang Hao

Queen Mary University of London, Mile End Road, London, E1 4NS, United Kingdom

yan.zhao@elec.qmul.ac.uk

Abstract: This paper proposes a radial dependent dispersive finite-difference time-domain method for the modelling of electromagnetic cloaking structures. The permittivity and permeability of the cloak are mapped to the Drude dispersion model and taken into account in dispersive FDTD simulations. Numerical simulations demonstrate that under ideal conditions, objects placed inside the cloak are 'invisible' to external electromagnetic fields. However for the simplified cloak based on linear transformations, the back scattering has a similar level to the case of a PEC cylinder without any cloak, rendering the object still being 'visible'. It is also demonstrated numerically that the simplified cloak based on high-order transformations can indeed improve the cloaking performance.

References and links

1. J. B. Pendry, D. Schurig, and D. R. Smith, "Controlling electromagnetic fields," Science **312**, 1780-1782 (2006).
2. V. G. Veselago, "The electrodynamics of substances with simultaneously negative value of ε and μ," Sov. Phys. Usp. **10**, 509 (1968).
3. S. A. Cummer, B.-I. Popa, D. Schurig, and D. R. Smith, "Full-wave simulations of electromagnetic cloaking structures," Phys. Rev. E **74**, 036621 (2006).
4. W. Cai, U. K. Chettiar, A. V. Kildishev, and V. M. Shalaev, "Optical cloaking with metamaterials," Nat. Photonics **1**, 224-227 (2007).
5. W. Cai, U. K. Chettiar, A. V. Kildishev, and V. M. Shalaev, "Nonmagnetic cloak with minimized scattering," Appl. Phys. Lett. **91**, 111105 (2007).
6. U. Leonhardt, "Optical conformal mapping," Science **312**, 1777-1780 (2006).
7. M. Tsang, and D. Psaltis, "Magnifying perfect lens and superlens design by coordinate transformation," Phys. Rev. B **77**, 035122 (2008).
8. H. Chen and C. T. Chan, "Transformation media that rotate electromagnetic fields," Appl. Phys. Lett. **90**, 241105 (2007).
9. M. Rahm, S. A. Cummer, D. Schurig, J. B. Pendry, and D. R. Smith, "Optical design of reflectionless complex media by finite embedded coordinate transformations," Phys. Rev. Lett. **100**, 063903 (2008).
10. Y. Luo, J. Zhang, L. Ran, H. Chen, and J. A. Kong, "Controlling the emission of electromagnetic sources by coordinate transformation," ArXiv.org:0712.3776v1 (2007).
11. D.-H. Kwon and D. H. Werner, "Two-dimensional eccentric elliptic electromagnetic cloaks," Appl. Phys. Lett. **92**, 013505 (2008).
12. S. A Cummer, and D. Schurig, "One path to acoustic cloaking," New Jour. Physics **9**, 45 (2007).
13. H. Chen, and C. T. Chan, "Acoustic cloaking in three dimensions using acoustic metamaterials," Appl. Phys. Lett. **91**, 183518 (2007).
14. Z. Ruan, M. Yan, C. W. Neff, and M. Qiu, "Ideal cylindrical cloak: perfect but sensitive to tiny perturbations," Phys. Rev. Lett. **99** 113903 (2007).

15. M. Yan, Z. Ruan, and M. Qiu, "Cylindrical invisibility cloak with simplified material parameters is inherently visible," Phys. Rev. Lett. **99**, 233901 (2007).
16. G. Isic, R. Gajic, B. Novakovic, Z. V. Popovic, and K. Hingerl, "Radiation and scattering from imperfect cylindrical electromagnetic cloaks," Opt. Express **16**, 1413-1422 (2008).
17. B. Zhang, H. Chen, B.-I. Wu, Y. Luo, L. Ran, and J. A. Kong, "Response of a cylindrical invisibility cloak to electromagnetic waves," Phys. Rev. B **76**, 121101 (2007).
18. Y. Huang, Y. Feng, T. Jiang, "Electromagnetic cloaking by layered structure of homogeneous isotropic materials," Opt. Express **15**, 11133-11141 (2007).
19. A. Greenleaf, Y. Kurylev, M. Lassas, and G. Uhlmann, "Improvement of cylindrical cloaking with the SHS lining," Opt. Express **15**, 12717-12734 (2007).
20. D. A. B. Miller, "On perfect cloaking," Opt. Express **14**, 12457-12466 (2006).
21. D. Schurig, J. J. Mock, B. J. Justice, S. A. Cummer, J. B. Pendry, A. F. Starr, and D. R. Smith, "Metamaterial electromagnetic cloak at microwave frequencies," Science **314**, 977-980 (2006).
22. I. I. Smolyaninov, Y. J. Hung, and C. C. Davis, "Electromagnetic cloaking in the visible frequency range," ArXiv.org:0709.2862v2 (2007).
23. A. Alu, and N. Engheta, "Achieving transparency with plasmonic and metamaterial coatings," Phys. Rev. E **72**, 016623 (2005).
24. M. G. Silveirinha, A. Alu, and N. Engheta, "Parallel-plate metamaterials for cloaking structures," Phys. Rev. E **75**, 036603 (2007).
25. G. W. Milton, and N. P. Nicorovici, "On the cloaking effects associated with anomalous localized resonance," Proc. R. Soc. A **462**, 3027-3059 (2006).
26. H. Cory, Y. Lee, and Y. Hao, "On the use of conjugate dielectric and metamaterial slabs as radomes," IET Microw. Antenna Propag. **1**, 137-143 (2007).
27. D. Schurig, J. B. Pendry, and D. R. Smith, "Calculation of material properties and ray tracing in transformation media," Opt. Express **14**, 9794-9804 (2006).
28. H. Chen, B.-I. Wu, B. Zhang, and J. A. Kong, "Electromagnetic wave interactions with a metamaterial cloak," Phys. Rev. Lett **99**, 063903 (2007).
29. R. Weder, "A rigorous time-domain analysis of fullwave electromagnetic cloaking (Invisibility)," ArXiv.org:0704.0248v4 (2007).
30. K. S. Yee, "Numerical solution of initial boundary value problems involving Maxwell's equations in isotropic media," IEEE Trans. Antennas Propgat. **14**, 302-307 (1966).
31. A. Taflove, *Computational Electrodynamics: The Finite-Difference Time-Domain Method*. 2nd ed., Norwood, MA: Artech House, 2000.
32. R. Luebbers, F. P. Hunsberger, K. Kunz, R. Standler, and M. Schneider, "A frequency-dependent finite-difference time-domain formulation for dispersive materials," IEEE Trans. Electromagn. Compat. **32**, 222-227 (1990).
33. O. P. Gandhi, B.-Q. Gao, and J.-Y. Chen, "A frequency-dependent finite-difference time-domain formulation for general dispersive media," IEEE Trans. Microwave Theory Tech. **41**, 658-664 (1993).
34. D. M. Sullivan, "Frequency-dependent FDTD methods using Z transforms," IEEE Trans. Antennas Propagat. **40**, 1223-1230 (1992).
35. F. B. Hildebrand, *Introduction to Numerical Analysis*. New York: Mc-Graw-Hill, 1956.
36. J.-Y. Lee, and N.-H. Myung, "Locally tensor conformal FDTD method for modelling arbitrary dielectric surfaces," Microw. Opt. Tech. Lett. **23**, 245-249 (1999).
37. J. R. Berenger, "A perfectly matched layer for the absorption of electromagnetic waves," J. Computat. Phys. **114**, 185 (1994).
38. Y. Zhao, P. A. Belov, and Y. Hao, "Accurate modelling of left-handed metamaterials using a finite-difference time-domain method with spatial averaging at the boundaries," Jour. Opt. A: Pure Appl. Opt. **9**, 468-475 (2007).
39. Y. Zhao, and Y. Hao, "Finite-difference time-domain study of guided modes in nano-plasmonic waveguides," IEEE Trans. Antennas Propag. **55**, 3070-3077 (2007).

1. Introduction

The widespread interest in the invisibility of objects has led to the recent development in electromagnetic cloaking structures. Pendry *et al.* proposed an electromagnetic material through which electromagnetic fields can be controlled and manipulated to propagate around its interior region like the flow of water [1], hence objects placed inside become 'invisible' to external electromagnetic fields. The proposed cloaking structure in [1] requires inhomogeneous and anisotropic media, with both permittivity and permeability independently controlled and radially dependent. The magnitudes of the relative permittivity and permeability of the perfect cloak are less than one, therefore it cannot be constructed using naturally existing materials. The

recent development of metamaterials [2] (artificially engineered structures with exotic electro-magnetic properties which cannot be obtained naturally) allows the control of material parameters with freedom, and hence the construction of such cloaking structures. However same as the negative-index metamaterials [2], the cloaking materials are inevitably dispersive and therefore band-limited. Furthermore, the complete set of material parameters proposed in [1] requires the control of all the components of permittivity and permeability of the material, making it difficult for practical realisation. It has been proposed to use reduced sets of material parameters for both transverse electric (TE) [3] and transverse magnetic (TM) [4] cases. The reduced set of material parameters for the TM case eliminates the dependence on the material's magnetic property, which is especially important for the realisation of the cloak in the optical frequency range due to the absence of optical magnetism in nature. However, considerable reflections occur because of the impedance mismatch at the outer boundary of such a simplified cloak. Under the assumption of the geometric optics, a high-order transformation has been proposed in [5] to improve the performance and minimise the scattering introduced by the cloak.

The development of Pendry's cloak is based on the coordinate transformation technique [1, 6], which has also evoked other research topics such as the design of magnifying perfect and super lenses [7], the transformation media that rotate electromagnetic fields [8], the design of reflectionless complex media for shifting and splitting optical beams [9], and the design of conformal antennas [10] etc. The spatial transformation technique has also been applied to anslyse eccentric elliptic cloaks [11] and for acoustic cloaking [12, 13]. Other theoretical studies of the cloaking structure include the sensitivity of an ideal cloak to tiny perturbations [14], the performance of the cylindrical cloaks with simplified material parameters [15, 16, 17], the realisation of cloaking using a concentric layered structure of homogeneous isotropic materials [18], the improvement of the cloaking performance using soft-and-hard surface lining [19], and the broadband cloaking using sensors and active sources near the surface of a region [20] etc. The experimental demonstration of a simplified cloak consisting of split-ring resonators (SRRs) has been reported in microwave frequencies [21]. For the optical frequency range, the cloak can be constructed by embedding silver wires in a dielectric medium [4], or using a gold-dielectric concentric layered structure [22].

It is worth mentioning that there exist different approaches to render objects invisible, for example, by canceling the dipolar scattering using plasmonic coatings [23, 24], and using a left-handed media (LHM) coating [25, 26]. However, the plasmonic coating approach is limited to the sub-wavelength scale of the object, and the coating depends on the geometry and material parameters of the object to be cloaked; the cloaking performance using LHM coating is affected by the objects placed inside. In comparison to these different approaches, Pendry's cloak is more general and can be applied to objects with any dimensions and under any wavelength condition.

The modelling of Pendry's invisible cloak has been performed by using both analytical and numerical methods. Besides the widely used coordinate transformation technique [1, 6, 7, 8, 9, 10, 11, 12, 13, 16, 27], a cylindrical wave expansion technique [14], and a method based on the full-wave Mie scattering model [28] have also been applied. In addition, the full-wave finite element method (FEM) based commercial simulation package COMSOL Multiphysics$^{\text{TM}}$ has been extensively used to model different cloaks and validate theoretical predictions [3, 4, 5, 11, 16] due to its ability of dealing with anisotropic and radial dependent material parameters. While most of the numerical simulations have been performed in the frequency domain, little attention has been paid to the time-domain analysis of the cloaks. Frequency domain techniques such as FEM may become inefficient when wideband solutions are needed. So far the only time-domain analysis of the cloak is presented in [29] using a time-dependent scattering theory. In this paper, we propose a dispersive finite-difference time-

domain (FDTD) method to deal with both the frequency and radial dependent permittivity and permeability of the cloak. Due to its simplicity in implementation and ability of treating anisotropic and inhomogeneous materials, the FDTD method has been extremely popular for the analysis of waveguides, transmission lines and antennas as well as the calculation of dispersion diagrams of photonic crystals in both microwave and optical communities. The aim of this paper is to provide a full-wave FDTD solution to assist the analysis, design and optimisation of the cloaking structures. To the authors' knowledge, it is the first time that the FDTD method is implemented to model cloaking structures.

2. Dispersive FDTD modelling of the cloaking structure

A complete set of material parameters of the ideal cloak is given by [1]:

$$\varepsilon_r = \mu_r = \frac{r - R_1}{r}, \qquad \varepsilon_\phi = \mu_\phi = \frac{r}{r - R_1}, \qquad \varepsilon_z = \mu_z = \left(\frac{R_2}{R_2 - R_1}\right)^2 \frac{r - R_1}{r}, \qquad (1)$$

where R_1 and R_2 are the inner and outer radius of the cloak, respectively. It can be easily identified from (1) that the ranges of permittivity and the permeability within the cloak are $\varepsilon_r, \mu_r \in [0, (R_2 - R_1)/R_2]$, $\varepsilon_\phi, \mu_\phi \in [R_2/(R_2 - R_1), \infty]$ and $\varepsilon_z, \mu_z \in [0, R_2/(R_2 - R_1)]$. Since the values of ε_r, μ_r, ε_z and μ_z are less than one, same as the case for the LHMs, the cloak cannot be directly modelled using the conventional FDTD method with constant material parameters (at one particular location r). However, one can map the material parameters using dispersive material models e.g. Drude model (taking ε_r as an example)

$$\varepsilon_r(\omega) = 1 - \frac{\omega_p^2}{\omega^2 - j\omega\gamma}, \qquad (2)$$

where ω_p and γ are the plasma and collision frequencies of the material, respectively. By varying the plasma frequency, the radial dependent material parameters (1) can be achieved. Note that in practise, the plasma frequency of the material depends on the periodicity of the SRRs [21] or wires [4], which varies along the radial direction. Furthermore, different dispersion models (e.g. Debye, Lorentz etc.) can be also considered for the modelling of the cloak, which will lead to slightly different FDTD formula from the following ones.

Since the conventional FDTD method [30, 31] deals with frequency-independent materials, the frequency-dependent FDTD method is hence referred as the dispersive FDTD method [32, 33, 34]. For simplicity, in this paper, we have implemented the dispersive FDTD method for a two-dimensional (2-D) case and only three field components are non-zero: E_x, E_y and H_z. The modelled cloak is cylindrical and infinite along z-direction ($\mu_r = \mu_\phi = \varepsilon_z = 0$ in (1)), however an extension to a three-dimensional (3-D) FDTD method to model a 3-D cloak [1] is straightforward. There are also different dispersive FDTD methods using different approaches to deal with frequency-dependent material parameters: the recursive convolution (RC) method [32], the auxiliary differential equation (ADE) method [33] and the Z-transform method [34]. Due to its simplicity, we have chosen the ADE method for the modelling of the cloak.

The ADE dispersive FDTD method is based on Faraday's and Ampere's Laws:

$$\nabla \times \mathbf{E} = -\frac{\partial \mathbf{B}}{\partial t}, \qquad (3)$$

$$\nabla \times \mathbf{H} = \frac{\partial \mathbf{D}}{\partial t}, \qquad (4)$$

as well as the constitutive relations $\mathbf{D} = \varepsilon\mathbf{E}$ and $\mathbf{B} = \mu\mathbf{H}$ where ε and μ are expressed by (1). Equations (3) and (4) can be discretised following a normal procedure [30, 31] which leads to

the conventional FDTD updating equations:

$$\mathbf{B}^{n+1} = \mathbf{B}^n - \Delta t \cdot \widetilde{\nabla} \times \mathbf{E}^{n+\frac{1}{2}}, \tag{5}$$

$$\mathbf{D}^{n+1} = \mathbf{D}^n + \Delta t \cdot \widetilde{\nabla} \times \mathbf{H}^{n+\frac{1}{2}}, \tag{6}$$

where $\widetilde{\nabla}$ is the discrete curl operator, Δt is the discrete FDTD time step and n is the number of the time steps.

In addition, auxiliary differential equations have to be taken into account and they can be discretised through the following steps. For the conventional Cartesian FDTD mesh, since the material parameters given in (1) are in cylindrical coordinates, the coordinate transformation

$$\begin{bmatrix} \varepsilon_{xx} & \varepsilon_{xy} \\ \varepsilon_{yx} & \varepsilon_{yy} \end{bmatrix} = \begin{bmatrix} \varepsilon_r \cos^2 \phi + \varepsilon_\phi \sin^2 \phi & (\varepsilon_r - \varepsilon_\phi) \sin \phi \cos \phi \\ (\varepsilon_r - \varepsilon_\phi) \sin \phi \cos \phi & \varepsilon_r \sin^2 \phi + \varepsilon_\phi \cos^2 \phi \end{bmatrix} \tag{7}$$

is used. The tensor form of the constitutive relation is given by

$$\varepsilon_0 \begin{bmatrix} \varepsilon_{xx} & \varepsilon_{xy} \\ \varepsilon_{yx} & \varepsilon_{yy} \end{bmatrix} \begin{bmatrix} E_x \\ E_y \end{bmatrix} = \begin{bmatrix} D_x \\ D_y \end{bmatrix} \quad \Leftrightarrow \quad \varepsilon_0 \begin{bmatrix} E_x \\ E_y \end{bmatrix} = \begin{bmatrix} \varepsilon_{xx} & \varepsilon_{xy} \\ \varepsilon_{yx} & \varepsilon_{yy} \end{bmatrix}^{-1} \begin{bmatrix} D_x \\ D_y \end{bmatrix}, \tag{8}$$

where

$$\begin{bmatrix} \varepsilon_{xx} & \varepsilon_{xy} \\ \varepsilon_{yx} & \varepsilon_{yy} \end{bmatrix}^{-1} = \frac{1}{\varepsilon_r \varepsilon_\phi} \begin{bmatrix} \varepsilon_r \sin^2 \phi + \varepsilon_\phi \cos^2 \phi & (\varepsilon_\phi - \varepsilon_r) \sin \phi \cos \phi \\ (\varepsilon_\phi - \varepsilon_r) \sin \phi \cos \phi & \varepsilon_r \cos^2 \phi + \varepsilon_\phi \sin^2 \phi \end{bmatrix}. \tag{9}$$

Note that the inverse of the permittivity tensor matrix exists only when $\varepsilon_r \neq 0$ and $\varepsilon_\phi \neq 0$, which is not the case for the inner boundary of the cloak. In our FDTD simulations, we place a perfect electric conductor (PEC) cylinder with radius equal to R_1 inside the cloak to guarantee the validity of (9).

Substituting (9) into (8) gives

$$\begin{cases} \varepsilon_r \varepsilon_\phi \varepsilon_0 E_x = (\varepsilon_r \sin^2 \phi + \varepsilon_\phi \cos^2 \phi) D_x + (\varepsilon_\phi - \varepsilon_r) \sin \phi \cos \phi D_y \\ \varepsilon_r \varepsilon_\phi \varepsilon_0 E_y = (\varepsilon_r \cos^2 \phi + \varepsilon_\phi \sin^2 \phi) D_y + (\varepsilon_\phi - \varepsilon_r) \sin \phi \cos \phi D_x \end{cases}, \tag{10}$$

Express ε_r in the Drude form of (1), Eq. (10) can be written as

$$\begin{cases} \varepsilon_0 \varepsilon_\phi \left(\omega^2 - j\omega\gamma - \omega_p^2 \right) E_x = \left[\left(\omega^2 - j\omega\gamma - \omega_p^2 \right) \sin^2 \phi + \varepsilon_\phi \left(\omega^2 - j\omega\gamma \right) \cos^2 \phi \right] D_x \\ \qquad\qquad + \left[\varepsilon_\phi \left(\omega^2 - j\omega\gamma \right) - \left(\omega^2 - j\omega\gamma - \omega_p^2 \right) \right] \sin \phi \cos \phi D_y, \\ \varepsilon_0 \varepsilon_\phi \left(\omega^2 - j\omega\gamma - \omega_p^2 \right) E_y = \left[\left(\omega^2 - j\omega\gamma - \omega_p^2 \right) \cos^2 \phi + \varepsilon_\phi \left(\omega^2 - j\omega\gamma \right) \sin^2 \phi \right] D_y \\ \qquad\qquad + \left[\varepsilon_\phi \left(\omega^2 - j\omega\gamma \right) - \left(\omega^2 - j\omega\gamma - \omega_p^2 \right) \right] \sin \phi \cos \phi D_x. \end{cases} \tag{11}$$

Notice that ε_ϕ remains in (11) because its value is always greater than one (except at the inner surface of the cloak) and can be directly used in conventional FDTD updating equations [30, 31]. Using an inverse Fourier transform and the following rules:

$$j\omega \to \frac{\partial}{\partial t}, \qquad \omega^2 \to -\frac{\partial^2}{\partial t^2}, \tag{12}$$

the first equation of (11) can be rewritten in the time domain as

$$\varepsilon_0 \varepsilon_\phi \left(\frac{\partial^2}{\partial t^2} + \gamma \frac{\partial}{\partial t} + \omega_p^2 \right) E_x = \left[\left(\frac{\partial^2}{\partial t^2} + \gamma \frac{\partial}{\partial t} + \omega_p^2 \right) \sin^2 \phi + \varepsilon_\phi \left(\frac{\partial^2}{\partial t^2} + \gamma \frac{\partial}{\partial t} \right) \cos^2 \phi \right] D_x$$
$$+ \left[\varepsilon_\phi \left(\frac{\partial^2}{\partial t^2} + \gamma \frac{\partial}{\partial t} \right) - \left(\frac{\partial^2}{\partial t^2} + \gamma \frac{\partial}{\partial t} + \omega_p^2 \right) \right] \sin \phi \cos \phi D_y. \tag{13}$$

The FDTD simulation domain is represented by an equally spaced 3-D grid with periods Δx, Δy and Δz along x-, y- and z-directions, respectively. For discretisation of Eq. (13), we use the central finite difference operators in time (δ_t and δ_t^2) and the central average operator with respect to time (μ_t and μ_t^2):

$$\frac{\partial^2}{\partial t^2} \rightarrow \frac{\delta_t^2}{(\Delta t)^2}, \qquad \frac{\partial}{\partial t} \rightarrow \frac{\delta_t}{\Delta t}\mu_t, \qquad \omega_p^2 \rightarrow \omega_p^2 \mu_t^2,$$

where the operators δ_t, δ_t^2, μ_t and μ_t^2 are defined as in [35]:

$$
\begin{aligned}
\delta_t \mathbf{F}|_{m_x,m_y,m_z}^n &\equiv \mathbf{F}|_{m_x,m_y,m_z}^{n+\frac{1}{2}} - \mathbf{F}|_{m_x,m_y,m_z}^{n-\frac{1}{2}}, \\
\delta_t^2 \mathbf{F}|_{m_x,m_y,m_z}^n &\equiv \mathbf{F}|_{m_x,m_y,m_z}^{n+1} - 2\mathbf{F}|_{m_x,m_y,m_z}^{n} + \mathbf{F}|_{m_x,m_y,m_z}^{n-1}, \\
\mu_t \mathbf{F}|_{m_x,m_y,m_z}^n &\equiv \frac{\mathbf{F}|_{m_x,m_y,m_z}^{n+\frac{1}{2}} + \mathbf{F}|_{m_x,m_y,m_z}^{n-\frac{1}{2}}}{2}, \\
\mu_t^2 \mathbf{F}|_{m_x,m_y,m_z}^n &\equiv \frac{\mathbf{F}|_{m_x,m_y,m_z}^{n+1} + 2\mathbf{F}|_{m_x,m_y,m_z}^{n} + \mathbf{F}|_{m_x,m_y,m_z}^{n-1}}{4}.
\end{aligned}
\tag{14}
$$

Here $\mathbf{F}$ represents field components and m_x, m_y, m_z are indices corresponding to a certain discretisation point in the FDTD domain. The discretised Eq. (13) reads

$$
\begin{aligned}
\varepsilon_0 \varepsilon_\phi \left[\frac{\delta_t^2}{(\Delta t)^2} + \gamma \frac{\delta_t}{\Delta t}\mu_t + \omega_p^2 \mu_t^2 \right] E_x &= \left\{ \left[\frac{\delta_t^2}{(\Delta t)^2} + \gamma \frac{\delta_t}{\Delta t}\mu_t + \omega_p^2 \mu_t^2 \right] \sin^2\phi \right. \\
&+ \varepsilon_\phi \left[\frac{\delta_t^2}{(\Delta t)^2} + \gamma \frac{\delta_t}{\Delta t}\mu_t \right] \cos^2\phi \right\} D_x + \left\{ \varepsilon_\phi \left[\frac{\delta_t^2}{(\Delta t)^2} + \gamma \frac{\delta_t}{\Delta t}\mu_t \right] \right. \\
&\left. - \left[\frac{\delta_t^2}{(\Delta t)^2} + \gamma \frac{\delta_t}{\Delta t}\mu_t + \omega_p^2 \mu_t^2 \right] \right\} \sin\phi \cos\phi D_y.
\end{aligned}
\tag{15}
$$

Note that in (15), the discretisation of the term ω_p^2 of (13) is performed using the central average operator μ_t^2 in order to guarantee an improved stability; the central average operator μ_t is used for the term containing γ to preserve the second-order feature of the equation. Equation (15) can be written as

$$
\begin{aligned}
\varepsilon_0 \varepsilon_\phi &\left[\frac{E_x^{n+1} - 2E_x^n + E_x^{n-1}}{(\Delta t)^2} + \gamma \frac{E_x^{n+1} - E_x^{n-1}}{2\Delta t} + \omega_p^2 \frac{E_x^{n+1} + 2E_x^n + E_x^{n-1}}{4} \right] \\
&= \sin^2\phi \left[\frac{D_x^{n+1} - 2D_x^n + D_x^{n-1}}{(\Delta t)^2} + \gamma \frac{D_x^{n+1} - D_x^{n-1}}{2\Delta t} + \omega_p^2 \frac{D_x^{n+1} + 2D_x^n + D_x^{n-1}}{4} \right] \\
&+ \varepsilon_\phi \cos^2\phi \left[\frac{D_x^{n+1} - 2D_x^n + D_x^{n-1}}{(\Delta t)^2} + \gamma \frac{D_x^{n+1} - D_x^{n-1}}{2\Delta t} \right] \\
&+ \sin\phi \cos\phi \left\{ \varepsilon_\phi \left[\frac{D_y^{n+1} - 2D_y^n + D_y^{n-1}}{(\Delta t)^2} + \gamma \frac{D_y^{n+1} - D_y^{n-1}}{2\Delta t} \right] \right. \\
&\left. - \left[\frac{D_y^{n+1} - 2D_y^n + D_y^{n-1}}{(\Delta t)^2} + \gamma \frac{D_y^{n+1} - D_y^{n-1}}{2\Delta t} + \omega_p^2 \frac{D_y^{n+1} + 2D_y^n + D_y^{n-1}}{4} \right] \right\}.
\end{aligned}
\tag{16}
$$

Therefore the updating equation for E_x can be obtained as

$$
E_x^{n+1} = \left[a_x D_x^{n+1} + b_x D_x^n + c_x D_x^{n-1} + d_x \overline{D_y}^{n+1} + e_x \overline{D_y}^{n} + f_x \overline{D_y}^{n-1} - \left(g_x E_x^n + h_x E_x^{n-1} \right) \right] / l_x.
\tag{17}
$$

where the coefficients a_x to l_x are given by

$$a_x = \sin^2\phi\left[\frac{1}{(\Delta t)^2} + \frac{\gamma}{2\Delta t} + \frac{\omega_p^2}{4}\right] + \varepsilon_\phi\cos^2\phi\left[\frac{1}{(\Delta t)^2} + \frac{\gamma}{2\Delta t}\right],$$

$$b_x = \sin^2\phi\left[-\frac{2}{(\Delta t)^2} + \frac{\omega_p^2}{2}\right] - \varepsilon_\phi\cos^2\phi\frac{2}{(\Delta t)^2},$$

$$c_x = \sin^2\phi\left[\frac{1}{(\Delta t)^2} - \frac{\gamma}{2\Delta t} + \frac{\omega_p^2}{4}\right] + \varepsilon_\phi\cos^2\phi\left[\frac{1}{(\Delta t)^2} - \frac{\gamma}{2\Delta t}\right],$$

$$d_x = \left\{\varepsilon_\phi\left[\frac{1}{(\Delta t)^2} + \frac{\gamma}{2\Delta t}\right] - \left[\frac{1}{(\Delta t)^2} + \frac{\gamma}{2\Delta t} + \frac{\omega_p^2}{4}\right]\right\}\sin\phi\cos\phi,$$

$$e_x = \left\{\varepsilon_\phi\left[-\frac{2}{(\Delta t)^2}\right] - \left[-\frac{2}{(\Delta t)^2} + \frac{\omega_p^2}{2}\right]\right\}\sin\phi\cos\phi,$$

$$f_x = \left\{\varepsilon_\phi\left[\frac{1}{(\Delta t)^2} - \frac{\gamma}{2\Delta t}\right] - \left[\frac{1}{(\Delta t)^2} - \frac{\gamma}{2\Delta t} + \frac{\omega_p^2}{4}\right]\right\}\sin\phi\cos\phi,$$

$$g_x = \varepsilon_0\varepsilon_\phi\left[-\frac{2}{(\Delta t)^2} + \frac{\omega_p^2}{2}\right], \quad h_x = \varepsilon_0\varepsilon_\phi\left[\frac{1}{(\Delta t)^2} - \frac{\gamma}{2\Delta t} + \frac{\omega_p^2}{4}\right], \quad l_x = \varepsilon_0\varepsilon_\phi\left[\frac{1}{(\Delta t)^2} + \frac{\gamma}{2\Delta t} + \frac{\omega_p^2}{4}\right].$$

Following the same procedure, the updating equation for E_y is

$$E_y^{n+1} = \left[a_y D_y^{n+1} + b_y D_y^n + c_y D_y^{n-1} + d_y\overline{D_x}^{n+1} + e_y\overline{D_x}^n + f_y\overline{D_x}^{n-1} - \left(g_y E_y^n + h_y E_y^{n-1}\right)\right]/l_y. \tag{18}$$

where the coefficients a_y to l_y are given by

$$a_y = \cos^2\phi\left[\frac{1}{(\Delta t)^2} + \frac{\gamma}{2\Delta t} + \frac{\omega_p^2}{4}\right] + \varepsilon_\phi\sin^2\phi\left[\frac{1}{(\Delta t)^2} + \frac{\gamma}{2\Delta t}\right],$$

$$b_y = \cos^2\phi\left[-\frac{2}{(\Delta t)^2} + \frac{\omega_p^2}{2}\right] - \varepsilon_\phi\sin^2\phi\frac{2}{(\Delta t)^2},$$

$$c_y = \cos^2\phi\left[\frac{1}{(\Delta t)^2} - \frac{\gamma}{2\Delta t} + \frac{\omega_p^2}{4}\right] + \varepsilon_\phi\sin^2\phi\left[\frac{1}{(\Delta t)^2} - \frac{\gamma}{2\Delta t}\right],$$

$$d_y = \left\{\varepsilon_\phi\left[\frac{1}{(\Delta t)^2} + \frac{\gamma}{2\Delta t}\right] - \left[\frac{1}{(\Delta t)^2} + \frac{\gamma}{2\Delta t} + \frac{\omega_p^2}{4}\right]\right\}\sin\phi\cos\phi,$$

$$e_y = \left\{\varepsilon_\phi\left[-\frac{2}{(\Delta t)^2}\right] - \left[-\frac{2}{(\Delta t)^2} + \frac{\omega_p^2}{2}\right]\right\}\sin\phi\cos\phi,$$

$$f_y = \left\{\varepsilon_\phi\left[\frac{1}{(\Delta t)^2} - \frac{\gamma}{2\Delta t}\right] - \left[\frac{1}{(\Delta t)^2} - \frac{\gamma}{2\Delta t} + \frac{\omega_p^2}{4}\right]\right\}\sin\phi\cos\phi,$$

$$g_y = \varepsilon_0\varepsilon_\phi\left[-\frac{2}{(\Delta t)^2} + \frac{\omega_p^2}{2}\right], \quad h_y = \varepsilon_0\varepsilon_\phi\left[\frac{1}{(\Delta t)^2} - \frac{\gamma}{2\Delta t} + \frac{\omega_p^2}{4}\right], \quad l_y = \varepsilon_0\varepsilon_\phi\left[\frac{1}{(\Delta t)^2} + \frac{\gamma}{2\Delta t} + \frac{\omega_p^2}{4}\right].$$

Note that the field quantities $\overline{D_x}$ in (18) and $\overline{D_y}$ in (17) are locally averaged values of D_x and D_y, respectively since the x- and y-components of the field are in different locations in the FDTD domain. The averaged values can be calculated using [36]

$$\overline{D_x}(i,j) = \frac{D_x(i,j) + D_x(i,j+1) + D_x(i-1,j) + D_x(i-1,j+1)}{4},$$

$$\overline{D_y}(i,j) = \frac{D_y(i,j) + D_y(i+1,j) + D_y(i,j-1) + D_y(i+1,j-1)}{4}, \tag{19}$$

where (i,j) is the coordinate of the field component.

The magnetic field H_z can be calculated starting from the constitutive relation $B_z = \mu_z H_z$, where μ_z is defined in (1). Again we map the permeability using the Drude model

$$\mu_z(\omega) = A\left(1 - \frac{\omega_{pm}^2}{\omega^2 - j\omega\gamma_m}\right), \tag{20}$$

where we choose $A = 2R_2/(R_2 - R_1)$, and ω_{pm} and γ_m are the magnetic plasma and collision frequencies of the material, respectively. Following the above discretisation procedure, the updating equation for H_z can be derived as

$$
\begin{aligned}
H_z^{n+1} &= \frac{1}{A}\left\{\left[\frac{1}{\mu_0(\Delta t)^2} + \frac{\gamma_m}{2\mu_0\Delta t}\right]B_z^{n+1} - \frac{2}{\mu_0(\Delta t)^2}B_z^n + \left[\frac{1}{\mu_0(\Delta t)^2} - \frac{\gamma_m}{2\mu_0\Delta t}\right]B_z^{n-1} \right. \\
&\left. + A\left[\frac{2}{(\Delta t)^2} - \frac{\omega_{pm}^2}{2}\right]H_z^n - A\left[\frac{1}{(\Delta t)^2} - \frac{\gamma_m}{2\Delta t} + \frac{\omega_{pm}^2}{4}\right]H_z^{n-1}\right\} \bigg/ \left[\frac{1}{(\Delta t)^2} + \frac{\gamma_m}{2\Delta t} + \frac{\omega_{pm}^2}{4}\right] . \tag{21}
\end{aligned}
$$

Equations (5), (6), (17), (18) and (21) form an FDTD updating equation set for the well-known leap-frog scheme [30].

Since the FDTD method is inherently a numerical technique, the spatial as well as time discretisations have important effects on the accuracy of simulation results. Also because the permittivity/permeability is frequency dependent, one can expect a slight difference between the analytical and numerical material parameters due to the discrete time step in FDTD. In general, for the modelling of conventional dielectrics with the relative permittivity/permeability greater than one, a spatial resolution (FDTD cell size) of $\Delta x < \lambda/10$ is required [31]. However from our previous analysis [38] that for the modelling of metamaterials especially LHMs, the numerical errors due to the time discretisation will cause spurious resonances, hence a requirement of $\Delta x < \lambda/80$ is necessary. For the case of the cloak, following the same approach as in [38] and for the case of plane-waves, substituting

$$\mathbf{E}^n = \mathbf{E}e^{jn\omega\Delta t}, \qquad \mathbf{D}^n = \mathbf{D}e^{jn\omega\Delta t}, \tag{22}$$

into Eq. (16), and comparing the resulting equation with the first equation of (10) one can find that $\widetilde{\varepsilon}_\phi$ (numerical permittivity along ϕ direction) has the exact analytical value, while $\widetilde{\varepsilon}_r$ (numerical permittivity along radial directions) takes the following form:

$$\widetilde{\varepsilon}_r = \varepsilon_0\left[1 - \frac{\omega_p^2(\Delta t)^2\cos^2\frac{\omega\Delta t}{2}}{2\sin\frac{\omega\Delta t}{2}\left(2\sin\frac{\omega\Delta t}{2} - j\gamma\Delta t\cos\frac{\omega\Delta t}{2}\right)}\right]. \tag{23}$$

Note that Eq. (23) simplifies to the Drude dispersion model (2) when $\Delta t \to 0$. We plot the comparison between the analytical (2) and numerical relative permittivity (23) for the case of $\varepsilon_r = 0.1$ (lossless) in Fig. 1. It is apparent that the conventional requirement of FDTD spatial resolution does not guarantee the accuracy for the modelling of the cloaks, and even for the case of $\Delta x = \lambda/40$, the numerical error is still about 2%.

With the expression of the numerical permittivity (23) available, one can correct the errors introduced by the discrepancy between numerical and analytical material parameters. For example, if the required permittivity is $\varepsilon_r = \varepsilon_r' + j\varepsilon_r''$, after simple derivations, the corrected plasma and collision frequencies can be calculated as

$$\widetilde{\omega_p}^2 = \frac{2\sin\frac{\omega\Delta t}{2}\left[-2(\varepsilon_r' - 1)\sin\frac{\omega\Delta t}{2} - \varepsilon_r''\gamma\Delta t\cos\frac{\omega\Delta t}{2}\right]}{(\Delta t)^2\cos^2\frac{\omega\Delta t}{2}}, \quad \widetilde{\gamma} = \frac{2\varepsilon_r''\sin\frac{\omega\Delta t}{2}}{(\varepsilon_r' - 1)\Delta t\cos\frac{\omega\Delta t}{2}}. \tag{24}$$
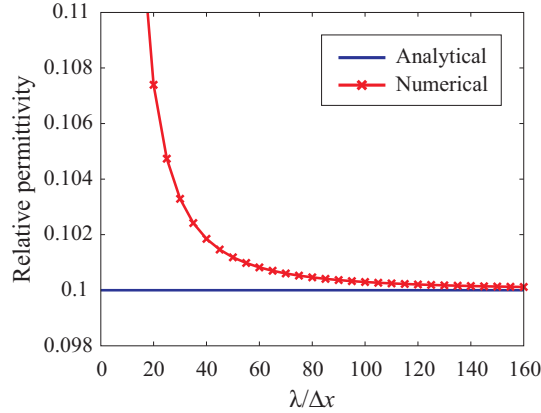
Fig. 1. The comparison between the analytical (2) and numerical material parameters (23) for different FDTD spatial resolutions for the case of $\varepsilon_r = 0.1$ (lossless).

It is found from our FDTD simulations with $\Delta x = \lambda/35$ that without the correction of numerical material parameters, the simulation becomes unstable before reaching the steady-state. The cause of such an instability is currently under our investigation. On the other hand, the correction of material parameters (both permittivity and permeability) guarantees stable FDTD simulations. Therefore in the following, the corrected material parameters (24) are always used.

3. Numerical results and discussion

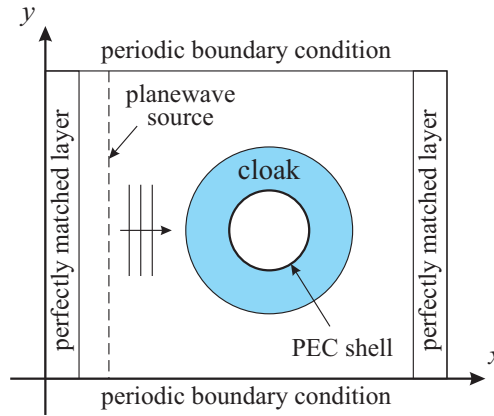The 2-D FDTD simulation domain is shown in Fig. 2. The following parameters are used in

Fig. 2. A two-dimensional (2-D) FDTD simulation domain for the case of plane-wave incidence on the cloak.

the simulations: FDTD cell size $\Delta x = \Delta y = \lambda/150$ where λ is the wavelength at the operating frequency $f = 2.0$ GHz, and the time step $\Delta t = \Delta x/\sqrt{2}c$, chosen according to the Courant stability criterion [31]. In the present paper, we assume the ideal lossless case i.e. the collision frequency in (2) is equal to zero ($\gamma = 0$). The radial dependent plasma frequency can be calculated using (24) with a given value of ε_r calculated from (1). The radii of the cloak are: $R_1 = 0.1$ m and $R_2 = 0.2$ m. The computation domain is truncated using Berenger's perfectly matched layer (PML) [37] in y-direction to absorb waves leaving the computation domain without intro-

ducing reflections, and terminated with the periodic boundary conditions (PBCs) in x-direction for the modelling of a plane-wave source. The plane-wave source is implemented by specifying a complete column of FDTD cells using a certain wave function (sinusoidal source in our case), see Fig. 2.

First we consider the ideal cloak, whose material parameters are given by (1) with $\mu_r = \mu_\phi = \varepsilon_z = 0$. Figure 3 shows the distributions of the electric and magnetic field components calculated from the dispersive FDTD simulation of the ideal cloak. Note that only the central
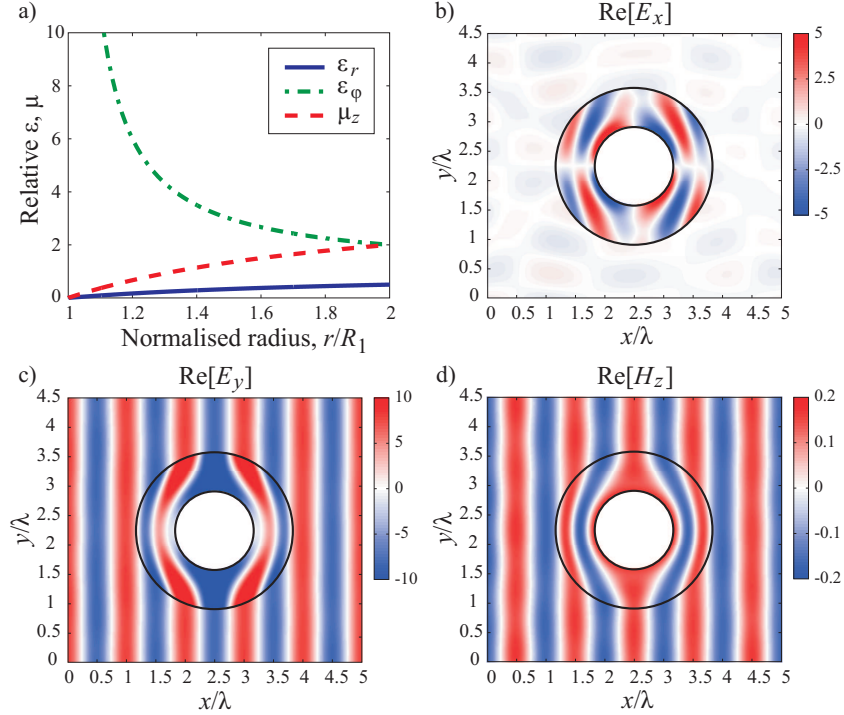

Fig. 3. (a) Material parameters for an infinite ideal cylindrical cloak [3] where all ε_r, ε_ϕ and μ_z are radial dependent. (b), (c) and (d) Field distributions from dispersive FDTD simulations of the cloak: (b) x-component of the electric field, (c) y-component of the electric field and (d) the magnetic field.

part of the simulation domain is shown and the actual computation domain is larger. It is seen in Fig. 3(b), (c) and (d) that the distribution is in good agreement with those in [3, 4] calculated using frequency domain methods, although there are tiny ripples in the magnetic field. In fact the field distribution presented in [3] shows even stronger ripples which may be due to the inadequate spatial resolution used in the calculation. These ripples are purely numerical and will disappear when an extremely fine FDTD grid is used. In our case, the slight ripples are also caused by the staircase approximation of the circular surface of the cloak in the Cartesian coordinate system. There are also non-zero scattered fields in the x-component of the electric field outside the cloak (see Fig. 3(b)), which is also a sign of numerical errors because an ideal cloak does not introduce any scattering outside the cloak. The staircase approximation only causes a very small amount of numerical errors due to the fine mesh used in our simulations. The staircase problem can be further alleviated to improve the accuracy of simulations using a conformal scheme in addition to the dispersive FDTD method i.e. using an effective permittivity at material boundaries, as it was done for the case of isotropic dispersive materials at planar

[38] and curved boundaries [39]. However, the difficulty lies in the anisotropy of the cloaking material, which leads to an eighth-order differential equation to be discretised (the order of the differential equation for the case of isotropic dispersive materials is four [39]).

As mentioned previously, it is difficult to realise the ideal cloak with all the components of permittivity and permeability being radial dependent. Therefore it is proposed in [4] that while keeping the same wave trajectory, a reduced set of material parameters also allows to construct a simplified cloak. The reduced set of material parameters is given by [4]:

$$\varepsilon_r = \left(\frac{R_2}{R_2 - R_1}\right)^2 \left(\frac{r - R_1}{r}\right)^2, \qquad \varepsilon_\phi = \left(\frac{R_2}{R_2 - R_1}\right)^2, \qquad \mu_z = 1. \qquad (25)$$

Following the same procedure, we have also modified the above proposed dispersive FDTD method to model the reduced set of material parameters and analysed its cloaking performance. The dimensions of the simplified cloak remain the same as the ideal one. The field distributions in the steady-state of the simulation are plotted in Fig. 4. Such a cloak significantly reduces
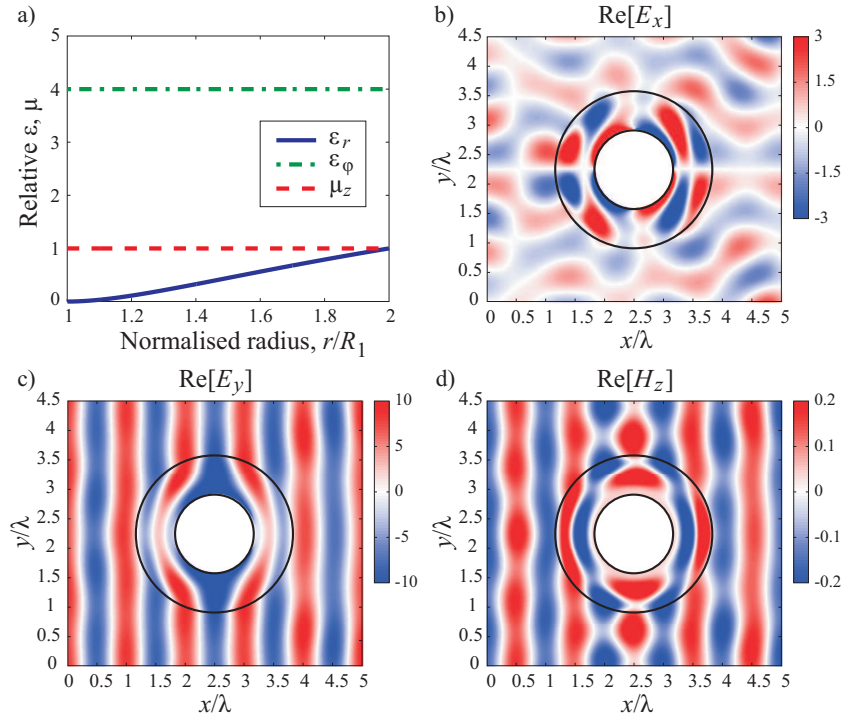

Fig. 4. (a) Material parameters for an infinite simplified cylindrical cloak using a linear transformation [4] where only ε_r is radial dependent. (b), (c) and (d) Field distributions from dispersive FDTD simulations of the cloak: (b) x-component of the electric field, (c) y-component of the electric field and (d) the magnetic field.

the complexity of practical realisation since only ε_r is radial dependent, as shown in Fig. 4(a). However, considerably reflections occur due to the fact that the impedance matching at the outer boundary of the simplified cloak is not satisfied anymore, see Fig. 4(b) and (d). Interestingly, the y-component of the electric field is only affected slightly by the scattered field. Note that here we only consider the simplified non-magnetic cloak [4], the simplified cloak proposed in [3] can be modelled in a similar way.

The scattering from the simplified cloak (25) due to the impedance mismatch can be reduced by using an improved cloak based on a high-order transformation [5]. The material parameters are given by [5]

$$\varepsilon_r = \left(\frac{r'}{r}\right)^2, \qquad \varepsilon_\phi = \left[\frac{\partial g(r')}{\partial r'}\right]^{-2}, \qquad \mu_z = 1. \tag{26}$$

where $r = g(r') = [(R_1/R_2)(r'/R_2 - 2) + 1]r' + R_1$. We have also modelled such a cloak and plotted the field distributions in Fig. 5. Its dimensions are kept the same as the previous two
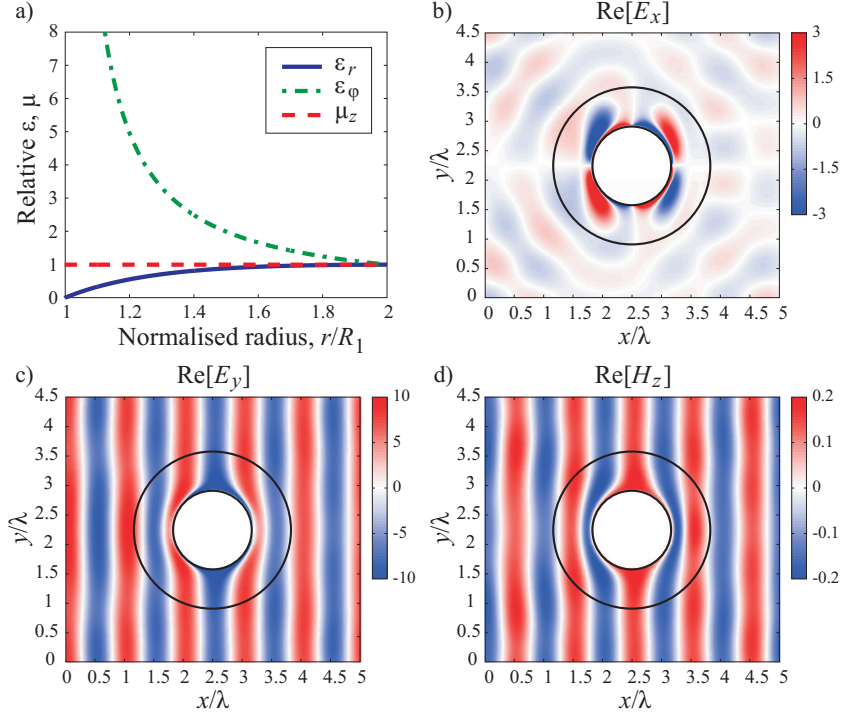

Fig. 5. (a) Material parameters for an infinite simplified cylindrical cloak using a high-order transformation [5] where only ε_r and ε_ϕ are radial dependent. (b), (c) and (d) Field distributions from dispersive FDTD simulations of the cloak: (b) x-component of the electric field, (c) y-component of the electric field and (d) the magnetic field.

cases. In fact the dimensions of this cloak is at its limit since it is required to have $R_1/R_2 < 0.5$ to guarantee a monotonic transformation [5]. The improved cloak adds an additional dependency of the permittivity on the radius, as shown in Fig. 5(a). It is clear that indeed the high-order transformation based cloak has an improved impedance on its outer boundary and hence considerably reduces the scattered field. Notice that the wavefront only starts to bend near the inner surface of the cloak, in comparison to the case for the ideal cloak shown in Fig. 3. This is due to the slow variance of the impedance from the outer boundary towards inside the cloak.

For demonstration, we have also plotted the power flow diagrams as well as the scattering patterns in Fig. 6 for the above ideal cloak, the simplified cloak based on a linear transformation, and the simplified cloak based on a the high-order transformation. The power flow diagrams show that for the ideal case (Fig. 6(a)), the wavefront enters the cloak smoothly, bends around the central region and returns to its original pattern after leaving the cloak. The cloak based on the high-order transformation (Fig. 6(c)) shows a similar pattern with a smooth bending of the wavefront near the central region of the cloak. However due to reflections, the power flow
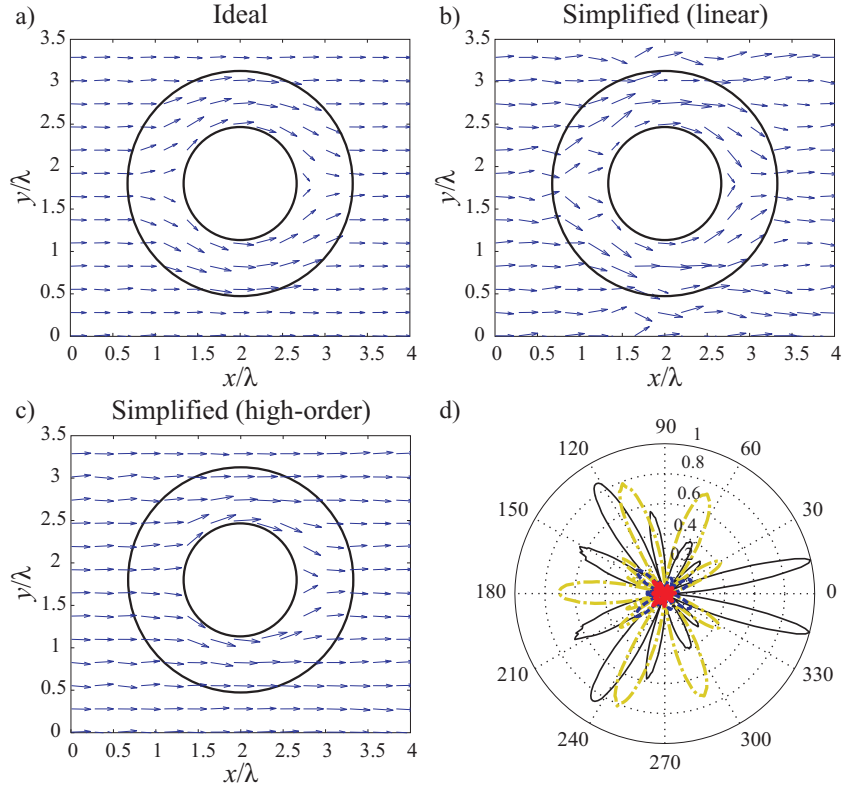
Fig. 6. Power flow diagrams for (a) the ideal cloak [3], (b) the simplified cloak based on the linear transformation [4] and (c) the simplified cloak based on a high-order transformation [5]. (d) Comparison of the scattering patterns for different cloaks and for the case of the PEC cylinder without cloak: black solid line - PEC cylinder; yellow dot-dashed line - linear transformation based simplified cloak; blue dashed line - high-order transformation based simplified cloak; red solid line - ideal cloak.

is disturbed before entering the cloak, while the wavefront leaving the cloak has a relatively smoother distribution. For the case of the cloak based on the linear transformation as shown in Fig. 6(b), the waves do not strictly follow the trend of the bending inside the cloak and propagate in arbitrary directions. The consequence is that the external field is significantly disturbed. This can be clearly identified from the scattering patterns. The scattering pattern is calculated with the reference to the free space case without any cloak or objects, and then normalised to the scattering pattern of a PEC cylinder without any cloak, see Fig. 6(d). For all the cloaks, the scattering at the back of the cloak (relative to the direction of wave incidence) is dramatically reduced. However the level of scattered field for the linear cloak is almost the same as the case for a PEC cylinder without any cloak, leading to the conclusion that the object placed inside this simplified cloak can be detected from its front side, similar to the conclusion drawn in [15]. For the high-order transformation based cloak, the scattering is reduced by around four times comparing with the linear transformation based one. Theoretically the ideal cloak has zero scattered field, however the nonzero (small) values in Fig. 6(d) is mainly caused by the staircase approximation in FDTD simulations, and will approach zero when an extremely fine FDTD grid is used or a conformal scheme is employed, as mentioned earlier.

4. Conclusion

In conclusion, we have proposed a dispersive FDTD method for the modelling of the cloaking structure. The unusual material parameters (the relative magnitudes of the permittivity and permeability are less than one) are mapped to the Drude dispersion model, which is then taken into account in FDTD simulations using an auxiliary differential equation based method. The proposed method is implemented in a two-dimensional case and three different cylindrical cloaks are considered in our simulations: the ideal cloak, the linear transformation based cloak and the high-order transformation based cloak. It is found from the simulations that the linear transformation based cloak introduces a level of back scattering similar to the one of a PEC cylinder without the cloak, causing the possibility of the object being detected. Such scattering can be significantly reduced by using the high-order transformation based cloak. In this paper we have only considered lossless cloaks. The 'ideal' cloak with a material loss of $\tan\delta = 0.1$ has been modelled in [3] using the finite element method, and the case for $\tan\delta = 0.01$, 0.1 and 1 modelled in [28] using a full-wave Mie scattering theory. Lossy cloaks can be also directly modelled using the above proposed dispersive FDTD method by specifying a certain value for the collision frequency in the Drude model for ε_r and defining a dielectric loss for ε_ϕ.